Reaction Pathways for the Oxidation of Methanol to Formaldehyde by an Iron−Oxo Species

Kazunari Yoshizawa* and Yoshihisa Kagawa

Department of Molecular Engineering, Kyoto University, Sakyo-ku, Kyoto 606-8501, Japan

Received: March 31, 2000; In Final Form: August 3, 2000

The reaction mechanism and energetics for the conversion of methanol to formaldehyde by an iron−oxo species, FeO^+, is investigated. Three competitive reaction pathways for the catalytic reaction are analyzed from DFT computations at the B3LYP level of theory. In Path 1, the H atom of the OH group of methanol is first abstracted by the oxo group of FeO^+ via a four-centered transition state (**TS_{1-1}**) leading to the intermediate complex $HO-Fe^+-OCH_3$, and after that one of the H atoms of the OCH_3 group is shifted to the OH ligand via a five-centered transition state (**TS_{1-2}**) to form the final product complex $H_2O-Fe^+-OCH_2$. In Path 2, one of the H atoms of the CH_3 group of methanol is abstracted by the oxo group via a five-centered transition state (**TS_{2-1}**) leading to the intermediate complex $HO-Fe^+-OHCH_2$, and then the H atom of the $OHCH_2$ group is shifted to the OH ligand via a four-centered transition state (**TS_{2-2}**) to give the product complex. Unlike Paths 1 and 2, which involve a hydrogen shift, the first step in Path 3 involves a methyl migration that takes place via a four-centered transition state (**TS_{3-1}**) resulting in the formation of the intermediate complex $HO-Fe^+-OCH_3$ and the second half of Path 3 is identical to that of Path 1. From B3LYP computations, Path 1 and Path 2 are competitive in energy and Path 3 is unlikely from the energetic viewpoint. Kinetic isotope effects (k_H/k_D) for the electronic processes of **TS_{1-1}**, **TS_{2-1}**, and **TS_{3-1}** are computed and analyzed.

Introduction

Alcohols are oxidized to aldehydes, carboxylic acids, ketones, and carbon oxides in solution by various transition-metal complexes that include Cr, Mn, Fe, and so on.[1] The functionalization of the C−H, O−H, and C−O bonds of alcohols by metal complexes is of recent interest in pure and applied chemistry.[2] Methanol is, of course, the smallest member of aliphatic alcohols and one of the most important industrial synthetic raw materials. A large variety of chemicals are now produced from methanol as a starting material. For example, formaldehyde is now manufactured directly from methanol via two different routes: (1) dehydrogenation or oxidative dehydrogenation in the presence of Ag or Cu catalysts, and (2) oxidation in the presence of Fe-containing MoO_3 catalysts.[3] Direct methanol fuel cells[4] present some distinct potential advantages over combustion engines and hydrogen fuel cells for transportation and remote power applications.[5] The decomposition of methanol on metal electrode surfaces has been extensively investigated in the field of electrochemistry,[6] mainly with the development of direct methanol fuel cells in mind. Formaldehyde is formed on anode surfaces in the first two-electron oxidation step ($CH_3OH \rightarrow CH_2O + 2H^+ + 2e^-$). Thus, the oxidation chemistry of methanol is rich considering its wide, potential applications in various fields.

The selective functionalization of the chemical bonds of small molecules by transition-metal catalysts or enzymes has also been a recent issue of discussion from a theoretochemical viewpoint, but our understanding is still limited especially with respect to the mechanistic and energetic aspects. Methanol has three kinds of strong bonds: the C−H, the O−H, and the C−O bonds, the dissociation energies of which are 94, 104, and 90 kcal/mol, respectively. It is of great importance to increase our knowledge concerning how the chemical bonds of methanol are activated and transformed by transition-metal complexes. In this article we demonstrate the mechanism for the conversion of methanol to formaldehyde by an iron−oxo species from density functional theory (DFT)[7] calculations. We place special emphasis on the research of possible reaction pathways and their energetics.

The Methanol−Formaldehyde Conversion by FeO^+

Schröder, Schwarz, and their collaborators have reported interesting gas-phase oxidation reactions of various molecules by bare transition-metal oxide ions, which frequently activate inert C−H bonds of substrate hydrocarbons in the initial stages of the reactions.[8] Their recent experimental studies have been performed with Fourier transform ion-cyclotron resonance (FTICR) mass spectrometry. One of the most important findings is, we think, the discovery of the reactivity of the bare FeO^+ complex and its potential applicability in considering the mechanistic aspects of catalytic or enzymatic chemistry; FeO^+ is able to cause the conversion of methane to methanol[9] and the conversion of benzene to phenol,[10] which are two of the most challenging issues in modern catalytic chemistry.[11] These gas-phase reactions are extremely important in that they may be viewed as simple model reactions for catalytic or enzymatic hydroxylations that are frequently mediated by iron−oxo complexes. Our theoretical analyses[12] have played a role in better understanding the mechanism for these basic gas-phase hydroxylation reactions.

Some mechanistic features observed in the reactions of FeO^+ with aliphatic alcohols under FTICR conditions were also reported by Schröder, Schwarz, and their collaborators.[13] Of course, FeO^+ can serve as an oxidant for the conversion of

* Author to whom correspondence should be addressed. E-mail: kazunari@scl.kyoto-u.ac.jp.

10.1021/jp0012552 CCC: $19.00
Published on Web 09/21/2000

SCHEME 1

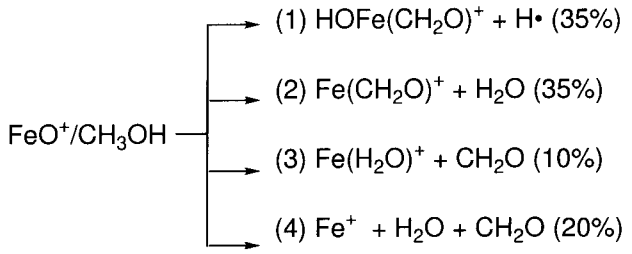

aliphatic alcohols to the corresponding aldehydes. Scheme 1 shows product branching ratios determined for the gas-phase reaction between FeO^+ and methanol; note that the formation of formaldehyde and its iron complexes predominantly occurs in this reaction. The $HO-Fe^+-OCH_3$ complex formed by an H-atom transfer from the OH group of substrate methanol to the oxo group of FeO^+ was predicted to play a role as a central intermediate. In contrast to the oxidation of methane by FeO^+ in which the reaction efficiency is only ca. 10%, this reaction exhibits 100% efficiency.

Allison and Ridge[14] reported that the reaction between Fe^+ and methanol gives $FeOH^+ + CH_3^\bullet$ but neither Co^+ nor Ni^+ reacts with methanol. Weil and Wilkins[15] demonstrated that the reaction of Au^+ with methanol leads to $AuH + CH_2OH^+$, and Huang, Holman, and Gross,[16] showed that the Fe^+ ion has no reactivity to methanol but the Mo^+ ion and methanol react to form $Mo(CH_2O)^+ + H_2$. According to the work of Schwarz's group,[17] neither $Fe(CH_3)^+$, $Fe(OCH_3)^+$, $Fe(OH)^+$, nor $Fe(C_2H_4)^+$ successfully converts methanol to formaldehyde in the gas phase. These experiments clearly suggest that oxidative dehydrogenation in the presence of FeO^+ plays an essential role in the conversion of methanol to formaldehyde in the gas phase. Thus, the formation of H_2O is likely to be an important, concomitant process. Apart from the mechanistic proposals from FTICR mass spectroscopic measurements,[13] let us consider from DFT computations how the reaction of FeO^+ with methanol proceeds to lead to the formation of formaldehyde or its iron complexes. We assume that the encounter complex $OFe^+(OHCH_3)$ should be formed in the initial stages of the reaction, as proposed.[13] This assumption is quite reasonable because the OH group of methanol is most likely to coordinate directly to the Fe^+ ion as a ligand. After the formation of the initial reactant complex, there are three possible reaction pathways, as indicated in Scheme 2.

In Path 1, the H atom of the OH group of methanol is first abstracted by the oxo group of FeO^+ via a four-centered transition state ($\mathbf{TS_{1-1}}$) to form the intermediate complex $HO-Fe^+-OCH_3$, and after that, one of the H atoms of the OCH_3 group is shifted to the OH ligand via a five-centered transition state ($\mathbf{TS_{1-2}}$) giving the final product complex $H_2O-Fe^+-OCH_2$. All the fragment species observed[13] can reasonably be explained to come from this complex. This reaction pathway, termed a 1,2-elimination of H atoms, has been supported on the basis of isotope labeling experiments.[13] In Path 2, one of the H atoms of the CH_3 group of methanol is abstracted by the oxo group via a five-centered transition state ($\mathbf{TS_{2-1}}$) to form the intermediate complex $HO-Fe^+-OHCH_2$, and then the H atom of the $OHCH_2$ group is shifted to the OH ligand via a four-centered transition state ($\mathbf{TS_{2-2}}$) resulting in the formation of the product complex $H_2O-Fe^+-OCH_2$. This reaction process can be termed a 2,1-elimination of H atoms. The things are reverse in Path 1 and Path 2; the difference in these competitive reaction pathways is in whether the H-atom transfer from the OH group of substrate methanol takes place in the first step or in the second step. Path 3 is clearly different from these two reaction pathways in mechanistic aspects; in the first step of this reaction pathway a methyl migration that takes place via a four-centered transition state ($\mathbf{TS_{3-1}}$) leads to the intermediate complex $HO-Fe^+-OCH_3$ and the second half of Path 3 is identical to that of Path 1.

Method of Calculation

We optimized local minima on the potential energy hypersurfaces corresponding to the reactant complex, the reaction intermediates, the final complex, and other fragment species using the hybrid (Hartree−Fock/density functional theory) B3LYP method.[18,19] It consists of the Slater exchange, the Hartree−Fock exchange, the exchange functional of Becke,[18] the correlation functional of Lee, Yang, and Parr (LYP),[19] and the correlation functional of Vosko, Wilk, and Nusair.[20] The spin-unrestricted version of this methodology was used for all

SCHEME 2

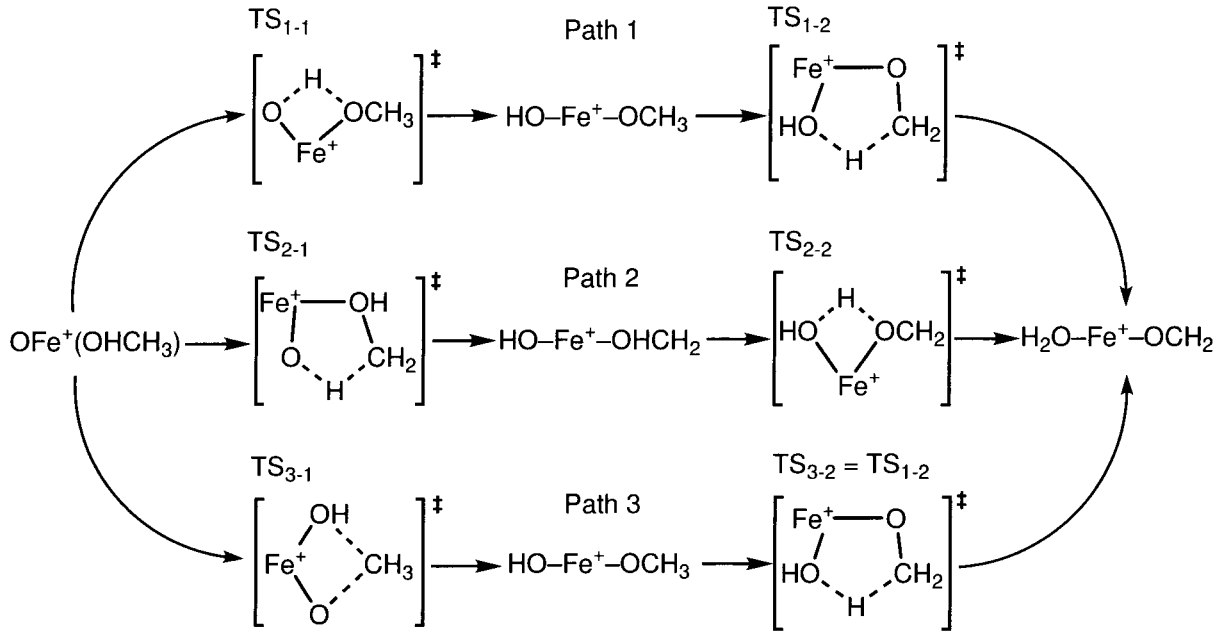

TABLE 1: Bond Distances (r_e in Å) and Dissociation Energies (D_e in kcal/mol) of the $^6\Sigma^+$ State of FeO^+ from Computations at Various Levels of Theory and from Experiment

method	basis set[a]	r_e	D_e
MP2(FC)	BSI	1.760[b]	40.8[b]
MP4(FC)	BSI	1.749[b]	44.2[b]
CISD+D(FC)	BSI	1.743[b]	33.6[b]
CCSD(T)(FC)	BSI	1.651[b]	64.7[b]
QCISD(T)(FC)	BSI	1.650[b]	72.2[b]
QCISD(T)(FC)	BSII	1.636[b]	74.6[b]
CASSCF	BSI	1.7[b]	25.4[b]
CASSCF	BSII	1.64[b]	28.7
MRCI+D(FC)	BSI	1.66[b]	70.2[b]
MRCI+D(FC)	BSII	1.64[b]	74.6[b]
CASPT2N(full)	BSI	1.64[b]	74.6[b]
CASPT2N(full)	BSII	1.64[b]	86.5[b]
B3LYP	6-311G**	1.632	75.2
experimental			81.4 ± 1.4[c]

[a] BSI: Contracted Gaussian basis sets (9s5d1d)/[4s2p1d] for oxygen and (14s10p6d1f)/[8s5p3d1f] for iron. BSII: Contracted Gaussian basis sets (14s9p4d3f)/[4s3p2d] for oxygen and (14s11p6d3f)/[8s7p4d1f] for iron. 6-311G**: see the text. [b] Cited from ref 25. [c] Cited from ref 26. There are no experimental data on the distance of FeO^+.

calculations. For the Fe atom we used the (14s9p5d) primitive set of Wachters[21] supplemented with one polarization f-function ($\alpha = 1.05$)[22] resulting in a (611111111|51111|311|1) [9s5p3d1f] contraction, and for the H, C, and O atoms we used the 6-311G** basis set of Pople and co-workers.[23] We referred to these as 6-311G** throughout this article. Transition-state structures were also optimized at the same level of theory. Vibrational analyses were systematically carried out in order to ensure that all optimized geometries correspond to a local minimum that has no imaginary frequency mode or a saddle point that has only one imaginary frequency mode. Zero-point vibrational energy corrections were taken into account in calculating the total energies of the reaction species. All DFT calculations were performed with the Gaussian 98 ab initio program package.[24] All the elementary electronic processes in the reaction pathways are reasonably assumed to take place in concerted manners. We list in Table 1 computed values for the dissociation energy of the $^6\Sigma^+$ state of FeO^+ at various levels of theory as well as an experimental value. The $^6S-{}^4G$ and $^6S-{}^2I$ splittings of Fe^{3+} are 91 and 134 kcal/mol, respectively;[27] these quantities were computed to be 115.3 and 123.4 kcal/mol, respectively, at the B3LYP/6-311G** level. The B3LYP method behaves well for these quantities to give values comparable to experimental values. Thus, this hybrid DFT method is appropriate for the subject of this paper, the reaction between FeO^+ and methanol.

Mechanism and Energetics for the Reaction Pathways

Path 1. Let us first look at the energetics for the conversion of methanol to formaldehyde that occurs along Path 1. Figure 1 shows computed energy diagrams for the sextet and the quartet reaction pathways. The general profile of these diagrams is downhill toward the product direction and thus the reaction is highly exothermic. We therefore expect that this reaction should easily take place. The ground $^6\Sigma^+$ state of FeO^+ was calculated to lie 8.4 kcal/mol below the first excited $^4\Delta$ state. The

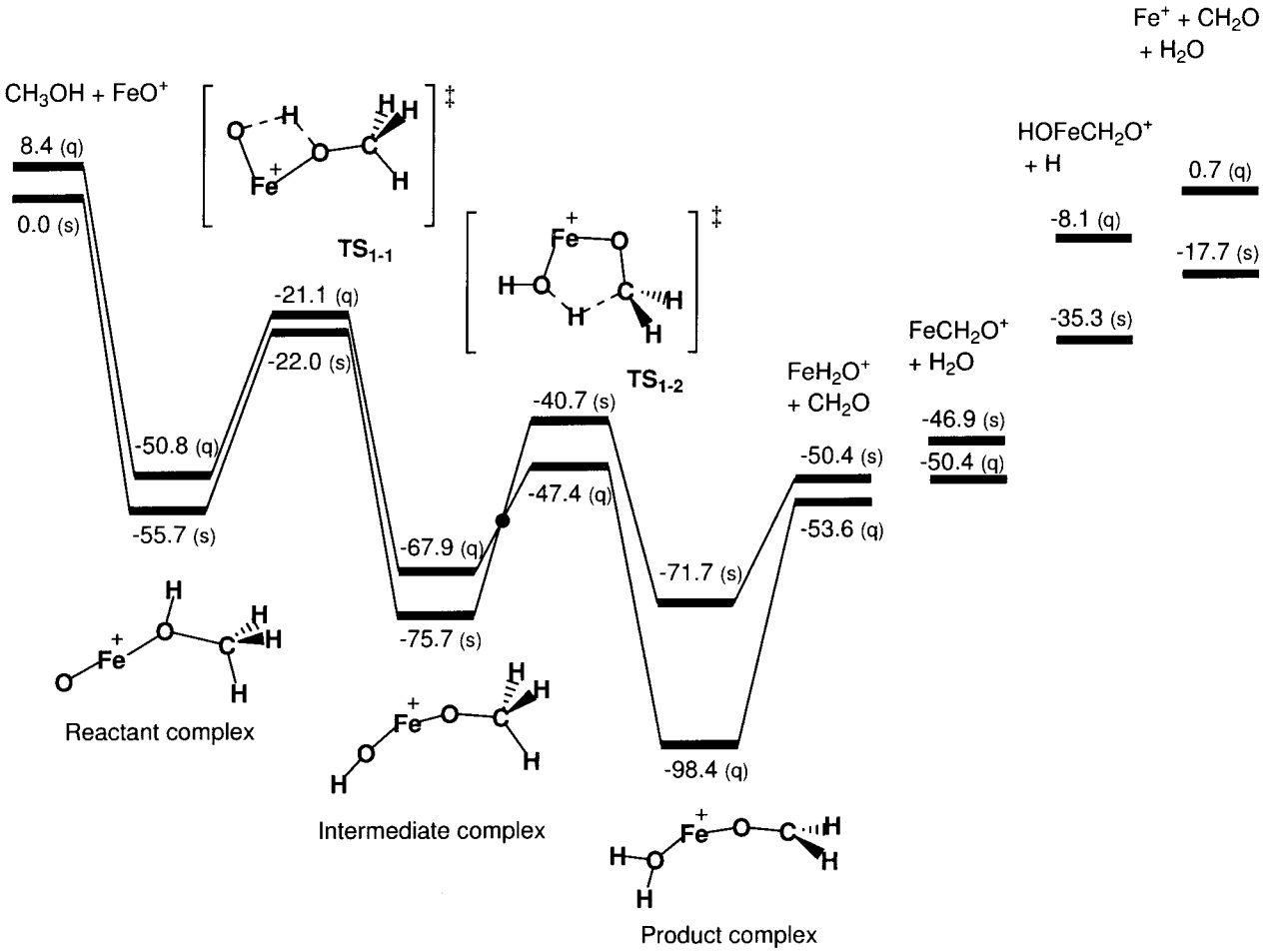

Figure 1. Computed energy diagrams for the conversion of methanol to formaldehyde by FeO^+ via Path 1 at the B3LYP/6-311G** level including zero-point vibrational energy corrections. Energies are in units of kcal/mol, and s and q in the parentheses indicate sextet and quartet, respectively.

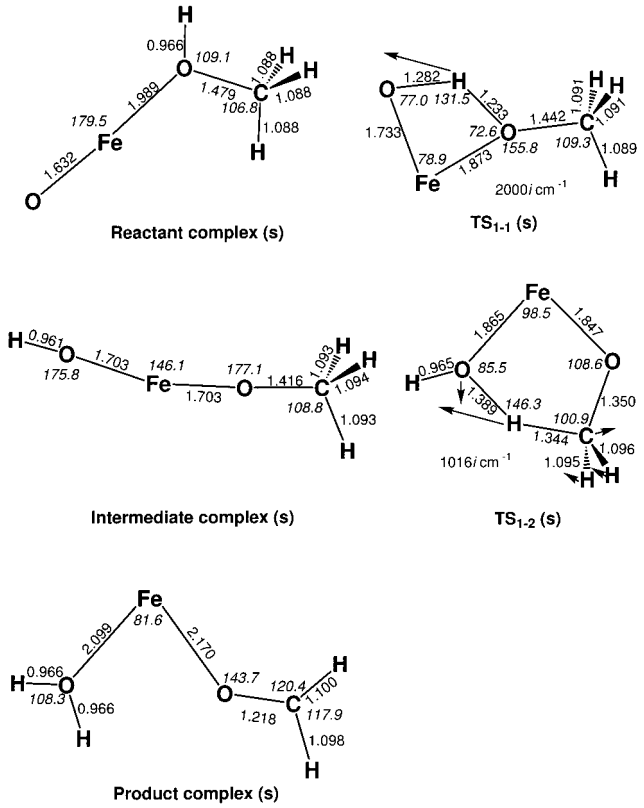

Figure 2. Optimized structures for the reaction species of the sextet state for the conversion of methanol to formaldehyde by FeO^+ via Path 1. Bond distances and angles (indicated in italic) are in units of Å and degree, respectively.

complexation between FeO^+ and methanol is highly exothermic—55.7 kcal/mol in the sextet state and 59.2 kcal/mol in the quartet state. The reacting system can pass over the transition state for the H atom abstraction from the OH group of methanol (**TS$_{1-2}$**) to form the intermediate complex $HO-Fe^+-OCH_3$ using this high complexation energy. This transition state lies well below the dissociation limit toward FeO^+ and methanol, and therefore the O−H bond should be easily cleaved.

In the second half of the reaction, one of the H atoms of the OCH_3 group migrates to the OH ligand via a five-centered transition state (**TS$_{1-2}$**) to form the final product complex $H_2O-Fe^+-OCH_2$. In sharp contrast to the first half of the reaction, the second half should not be spin-conserving. Since the sextet and the quartet states have very similar geometries, as mentioned later, our calculations strongly suggest a crossing between the two energy diagrams just in prior to **TS$_{1-2}$** and therefore a spin inversion, an nonadiabatic electronic process, is expected to occur from the sextet state to the quartet state in the vicinity of the crossing seam of the two potential energy surfaces. Since the transition state of the quartet state lies 6.7 kcal/mol below that of the sextet state, the energy barrier should be lowered by this quantity if the spin inversion takes place in the course of this electronic process. Therefore the spin inversion would play an important role in this electronic process. The resultant product complex, the ground state of which is a quartet, lies 98.4 kcal/mol below the dissociation limit of the sextet state and thus Path 1 is highly exothermic.

Figure 1 also presents computed energetics for the observed fragment species indicated in Scheme 1. Fragmentation (1) can derive from both the intermediate complex $HO-Fe^+-OCH_3$ and the product complex $H_2O-Fe^+-OCH_2$, but it would be natural to consider that fragmentations (2), (3), and (4) should exclusively come from the product complex $H_2O-Fe^+-OCH_2$.

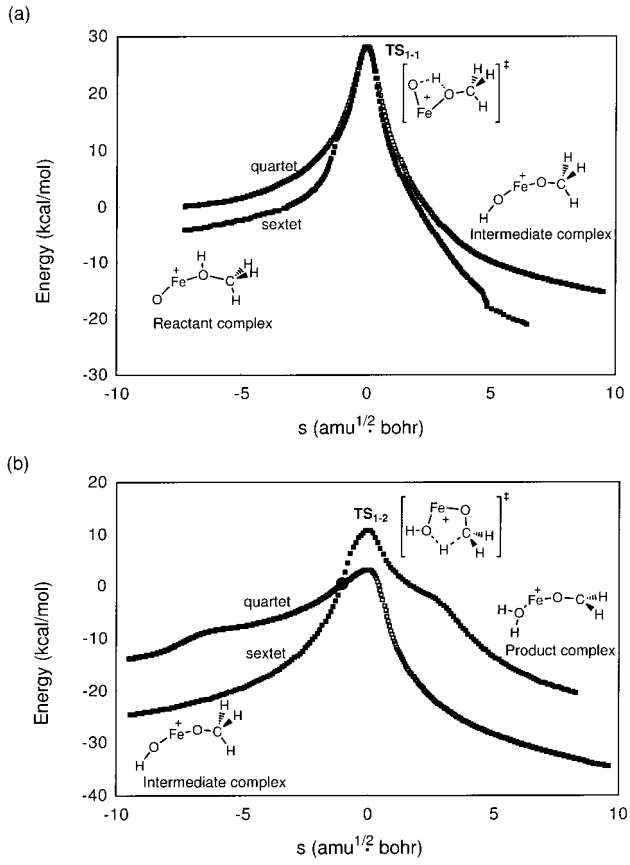

Figure 3. Energy profiles along the IRCs of Path 1 at the B3LYP/6-311G** level. Strictly speaking, the reaction coordinates (*s*) are slightly different for the sextet and the quartet energy profiles. Zero-point vibrational energy corrections are not included in the profiles.

As mentioned earlier, this reaction exhibits 100% efficiency. Since the energy diagrams are highly exothermic toward the product complex direction, the reacting system should acquire much energy if these elementary processes take place in the gas phase without any interaction with external fields. Such energy can be partly distributed to the fragmentations of the molecular system accordingly. It is of great interest that the total energy of each fragmentation is less than or nearly equal to the dissociation limit toward FeO^+ and methanol. We believe that the distribution of the fragment species indicated in Scheme 1 should be determined by the energy balance of the molecular system before and after the reaction. The energy that the reacting system acquires can be used for the generation of high-energy species such as $HOFe(CH_2O)^+ + H^\bullet$. As a result, fragmentation (1) is not minor (35% yield) despite its high potential energy. This presumption will be confirmed by dynamics calculations in our future work.

Optimized geometries of the reaction intermediates and the transition states of the sextet state are shown in Figure 2. Transition vectors and corresponding imaginary frequencies in the transition state structures are indicated. Since the difference between the geometries of the sextet state and the quartet state is small, we do not refer to the geometries of the quartet state, which the reader can see in Supporting Information 1. **TS$_{1-1}$** and **TS$_{1-2}$** are typical four- and five-centered transition states, respectively, that are responsible for a concerted H atom abstraction. The O−H bonds being dissociated and formed in **TS$_{1-1}$** are nearly equal in length; 1.233 and 1.282 Å, respectively. In **TS$_{1-2}$**, the distance of the C−H bond being dissociated is also close to that of the O−H bond being formed; 1.344 and 1.389 Å, respectively.

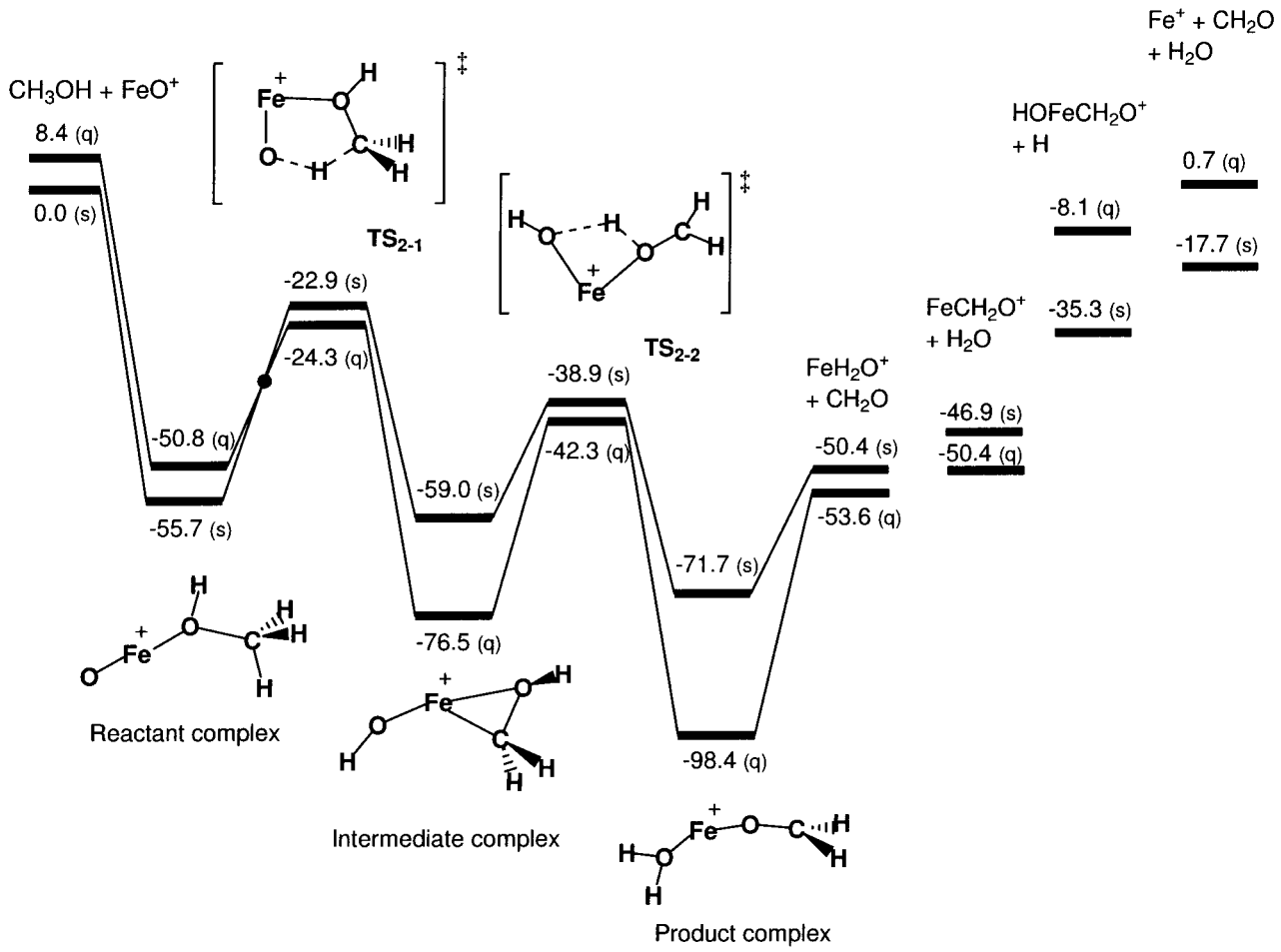

Figure 4. Computed energy diagrams for the conversion of methanol to formaldehyde by FeO^+ via Path 2 at the B3LYP/6-311G** level including zero-point vibrational energy corrections. Energies are in units of kcal/mol, and s and q in the parentheses indicate sextet and quartet, respectively.

Figure 3 presents energy profiles along the intrinsic reaction coordinates (IRCs)[28] for the first and the second halves of Path 1. IRC is the steepest descent path that connects a reactant and a product via a transition state on a potential energy surface. Strictly speaking, the reaction coordinates (s) are slightly different for the sextet and the quartet energy profiles. It is confirmed from these IRC analyses that $\mathbf{TS_{1-1}}$ and $\mathbf{TS_{1-2}}$ correctly connect the entire reaction pathway for the conversion of methanol to formaldehyde. Our IRC analyses suggest the existence of a crossing point between the sextet and the quartet energy profiles, as shown in the lower illustration of Figure 3; thus, the reacting system preferentially goes on the sextet potential energy surface in the first half of the reaction and on the quartet potential energy surface in the second half of the reaction. Such a spin inversion that can occur in the vicinity of the crossing region should play an essential role in transition-metal-catalyzed reactions.[29]

Let us first look at the IRC analysis on the first half of the reaction pathway from the reactant complex to the intermediate complex via $\mathbf{TS_{1-1}}$. This process can be viewed as a concerted 1,3-hydrogen migration. This is the most important step in which the O−H bond of the bound methanol is cleaved to migrate toward the ferryl oxygen, leading to the intermediate complex that incorporates resultant OH and OCH_3 ligands. The IRCs were traced from $\mathbf{TS_{1-1}}$ ($s = 0$), which has an imaginary vibrational mode of 2000i and 1869i cm^{-1} in the sextet and the quartet states, respectively, toward both reactant ($s < 0$) and product ($s > 0$) directions. The sharp energy peaks are a result of the high frequencies, and vice versa. Any such reaction pathway of steepest descent would, in principle, lead to an energy minimum in reactant or product "valleys".[28] Our IRC analyses successfully lead to the true local minimum points for both reactant and intermediate complexes. An important aspect along this reaction pathway is the cleavage of the O−H bond of methanol and the formation of a new O−H bond. The migrating hydrogen atom interacts not only with the two O atoms but also, to some extent, with the Fe ion. Thus, the Fe ion is not a spectator in this concerted process but can significantly contribute to the migration of the H atom. The Fe−H distance of $\mathbf{TS_{1-1}}$ is 1.909 and 1.880 Å in the sextet and the quartet states, respectively.[30] Taking these short distances into consideration, there is clearly orbital overlap between the migrating hydrogen atom and the Fe ion in the vicinity of the transition state. Thus, the Fe ion should play a role in this concerted electronic process.

Let us next look at the IRC analyses for the second half of the reaction pathway, in which the formation of the product complex occurs in a concerted manner via a 1,4-hydrogen migration. A remarkable aspect in this electronic process is the dissociation of the C−H bond and the formation of an O−H bond, resulting in the product complex that involves CH_2O and H_2O ligands. Judging from the five-centered transition state, the Fe ion is unlikely to play a central role in this concerted electronic process compared to the first half of the reaction via $\mathbf{TS_{1-1}}$. The IRCs were again traced from $\mathbf{TS_{1-2}}$ ($s = 0$), which has an imaginary vibrational mode of 1016i and 789i cm^{-1} in the sextet and the quartet states, respectively, toward both reactant ($s < 0$) and product ($s > 0$) directions. Since the imaginary frequencies of $\mathbf{TS_{1-2}}$ are nearly as half as those of $\mathbf{TS_{1-1}}$, the peaks of $\mathbf{TS_{1-2}}$ look relatively blunt.

Path 2. Figure 4 shows computed energy diagrams for Path 2. The five-centered transition state in Path 2 ($\mathbf{TS_{2-1}}$), the transition state for the abstraction of one of the H atoms of the CH_3 group of methanol, lies about 2 kcal/mol below the four-centered transition state in Path 1 ($\mathbf{TS_{1-1}}$), the transition state for the H atom abstraction of the OH group of methanol. Thus, $\mathbf{TS_{1-1}}$ and $\mathbf{TS_{2-1}}$ are very competitive from the energetic point of view. We find a crossing between the two energy diagrams before $\mathbf{TS_{2-1}}$ and therefore expect that a spin inversion should occur from the sextet state to the quartet state in the vicinity of this crossing point. However, since the sextet and the quartet states of $\mathbf{TS_{2-1}}$ are close in energy, this spin inversion would not produce a significant result with respect to the energetics of this electronic process. A similar crossing was found to occur during the C−H bond cleavage in the FeO^+/CH_4 system;[12a−d] in this process the spin inversion plays an essential role for a decrease in the activation barrier for the C−H bond cleavage of methane. Interestingly, there is a crossing of the sextet and the quartet potential energy surfaces only in the course of the C−H bond cleavage process in both Path 1 and Path 2. The first electronic process of Path 2 is easily accessible using the large complexation energy of the reactant complex, forming the resultant intermediate complex $HO-Fe^+-OHCH_2$. In contrast to the intermediate complex $HO-Fe^+-OCH_3$ in Path 1, the ground state of $HO-Fe^+-OHCH_2$ is a quartet. However, the energies of the ground states of both intermediates are accidentally nearly equal.

The second half of Path 2 is spin-conserving; the reacting system should move preferentially along the reaction pathway of the quartet state. The H atom of the OH group is abstracted via the four-centered transition state $\mathbf{TS_{2-2}}$ to form a water ligand. The barrier height for $\mathbf{TS_{2-2}}$ is 34.2 kcal/mol on the quartet surface, but it is easily accessible from the energetic point of view because $\mathbf{TS_{2-2}}$ is about 40 kcal/mol below the dissociation limit. All the observed fragment species indicated in Scheme 1 are also reasonably derived from this reaction pathway. We can therefore conclude that both Path 1 and Path 2 are likely to occur without collisions in the viewpoints of the energetics and the observed fragment species.

Optimized geometries of the reaction intermediates and the transition states of the sextet state in Path 2 are shown in Figure 5. The reader can see the geometries of the quartet state in Supporting Information 2. The things are reverse in Path 1 and Path 2, as mentioned above, and therefore the five-centered $\mathbf{TS_{2-1}}$ is similar to $\mathbf{TS_{1-2}}$ and the four-centered $\mathbf{TS_{2-2}}$ is similar to $\mathbf{TS_{1-1}}$ in essential bonding characters. However, we find from a close inspection of $\mathbf{TS_{2-2}}$ that the O−H bond being dissociated (1.009 Å) is much shorter than the O−H bond being formed (1.648 Å). Thus, this electronic process is not symmetric. The optimized structure of the intermediate complex $HO-Fe^+-OHCH_2$ is intriguing in that it involves a three-membered ring structure. Since the C−O bond of 1.431 Å is rather long and the Fe−C bond of 2.029 Å is a typical coordinate bond, this complex may be viewed as the three-coordinate complex $Fe^+(OH)_2(CH_2)$.

Path 3. Computed energy diagrams for Path 3 are shown in Figure 6. Note that the second half of this reaction pathway is identical to that of Path 1, as mentioned earlier. The transition state for the methyl migration ($\mathbf{TS_{3-1}}$) is comparable in energy to the dissociation limit toward FeO^+ and methanol, and its activation energy measured from the reactant complex is 53.1 and 51.0 kcal/mol on the sextet and the quartet potential energy surfaces, respectively. This transition state is unfavorable in energy compared to $\mathbf{TS_{1-1}}$ in Path 1 and $\mathbf{TS_{2-1}}$ in Path 2, but

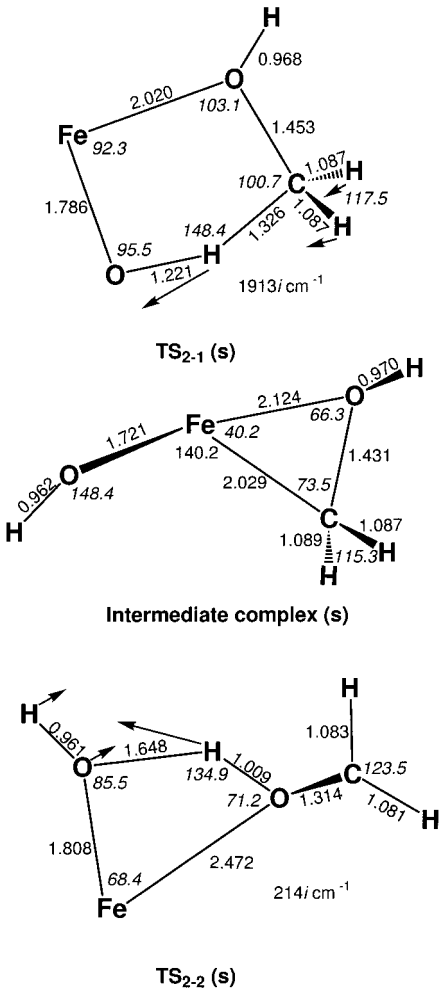

Figure 5. Optimized structures for the reaction species of the sextet state for the conversion of methanol to formaldehyde by FeO^+ via Path 2. Bond distances and angles (indicated in italic) are in units of Å and degree, respectively.

one cannot rule out the occurrence of Path 3 even if our discussion is restricted to high-vacuum gas-phase reactions. Any available kinetic energy can allow Path 3 to proceed.

An optimized geometry of the four-centered transition state $\mathbf{TS_{3-1}}$ of the sextet state in Path 3 is shown in Figure 7. The C−O bonds being cleaved and formed are 2.426 and 2.809 Å in length, respectively; thus, the migrating methyl group is nearly isolated. In this aspect, $\mathbf{TS_{3-1}}$ is remarkably different from $\mathbf{TS_{1-1}}$ and $\mathbf{TS_{2-1}}$. The reader can see a similar four-centered transition state of the quartet state in Supporting Information 3.

Energetics for the Observed Fragment Species. Let us finally look at the energetics for the fragment species generated in the gas phase. Computed enthalpies ΔH_f (in kcal/mol) for the formation of the fragment species at 298 K (1) $HOFe(CH_2O)^+ + H^\bullet$, (2) $Fe(CH_2O)^+ + H_2O$, (3) $Fe(H_2O)^+ + CH_2O$, and (4) $Fe^+ + H_2O + CH_2O$ are listed in Table 2. Since the ground state of FeO^+ is a spin sextet, it is reasonable to consider the enthalpy of $FeO^+(^6\Sigma^+) + CH_3OH(^1A')$ as a standard. Calculated enthalpy changes between the reactants and the products, $FeO^+ + CH_3OH \rightarrow Fe^+ + CH_2O + H_2O$, are −16.8 kcal/mol in the sextet state and −9.6 kcal/mol in the quartet state, being in good agreement with an experimental value obtained from Cooks' method, −14 kcal/mol. Even if we confine our discussion on the reaction pathway of the sextet state, the computed enthalpies are in fairly good agreement with the reported values[13] concerning the fragmentations (2), (3), and

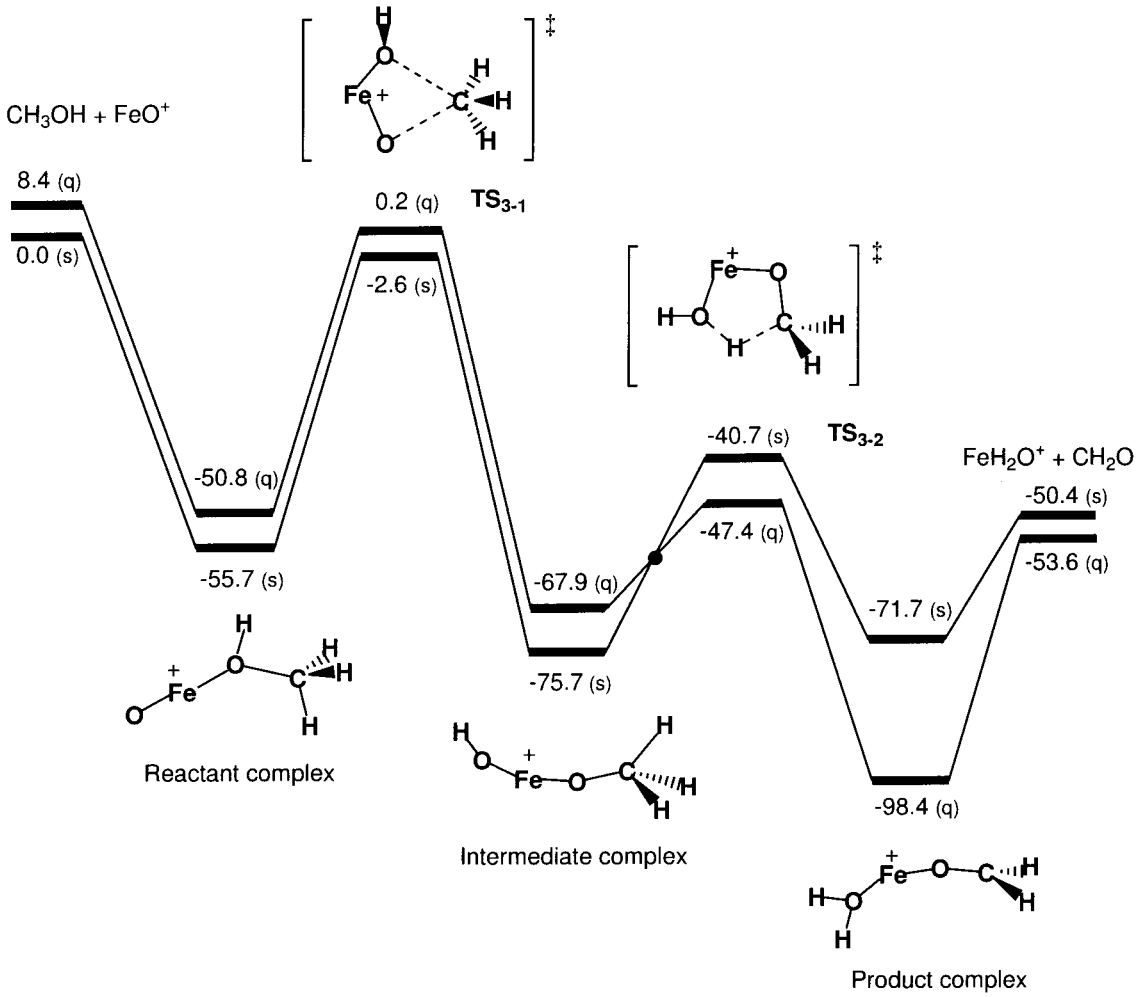

Figure 6. Computed energy diagrams for the conversion of methanol to formaldehyde by FeO^+ via Path 3 at the B3LYP/6-311G** level including zero-point vibrational energy corrections. Energies are in units of kcal/mol, and s and q in the parentheses indicate sextet and quartet, respectively. The second half of this reaction pathway is identical to that of Path 1.

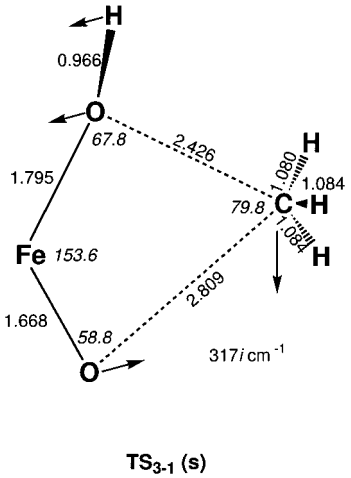

Figure 7. An optimized structure for $\mathbf{TS_{3-1}}$ of the sextet state for the conversion of methanol to formaldehyde by FeO^+ via Path 3. Bond distances and angles (indicated in italic) are in units of Å and degree, respectively.

(4). However, our computational results and the reported value for the fragmentation (1) are not in agreement. This inconsistency may derive from the simple additivity scheme used in ref 13, in which cooperative effects of two ligands were neglected. This presumption may be correct because of the fact that in the generated fragment species $HOFe(CH_2O)^+$ is the sole reaction species involving two ligands.

Kinetic Isotope Effects

Kinetic isotope effect (k_H/k_D) is an important measure in discussing how the electronic process for H atom abstraction of substrate hydrocarbon takes place in catalytic and enzymatic reactions. In this section, we consider the isotope effects in the FeO^+/CH_3OH system, concerning the electronic process associated with the first transition state in each reaction pathway. The kinetic isotope effects were obtained from the transition-state theory,[31] with the following expression:

$$\frac{k_H}{k_D} = \left(\frac{m^R_{D-form}\, m^{\#}_{H-form}}{m^R_{H-form}\, m^{\#}_{D-form}}\right)^{3/2} \left(\frac{I^R_{x_{D-form}} I^R_{y_{D-form}} I^R_{z_{D-form}}}{I^R_{x_{H-form}} I^R_{y_{H-form}} I^R_{z_{H-form}}}\right)^{1/2} \times \left(\frac{I^{\#}_{x_{H-form}} I^{\#}_{y_{H-form}} I^{\#}_{z_{H-form}}}{I^{\#}_{x_{D-form}} I^{\#}_{y_{D-form}} I^{\#}_{z_{D-form}}}\right)^{1/2} \frac{q^R_{\upsilon_{D-form}} q^{\#}_{\upsilon_{H-form}}}{q^R_{\upsilon_{H-form}} q^{\#}_{\upsilon_{D-form}}} \times \exp\left(-\frac{E^{\#}_{H-form} - E^{\#}_{D-form}}{RT}\right) \quad (1)$$

where the superscripts *R* and # specify the reactant complex and the transition state, respectively, for the molecular mass *m*,

TABLE 2: Measured Enthalpies and Calculated Enthalpies at 298 K ΔH_f (in kcal/mol) for the Formation of the Fragment Species (1) $HOFe(CH_2O)^+ + H^\bullet$, (2) $Fe(CH_2O)^+ + H_2O$, (3) $Fe(H_2O)^+ + CH_2O$, and (4) $Fe^+ + H_2O + CH_2O$

	$HOFe(CH_2O)^+ + H^\bullet$	$Fe(CH_2O)^+ + H_2O$	$Fe(H_2O)^+ + CH_2O$	$Fe^+ + H_2O + CH_2O$
ΔH_f	−11[a]	−47[a]	−45[a]	−14[a]
ΔH_f (sextet)	−33.7	−44.6	−49.8	−16.8
ΔH_f (quartet)	−14.9	−57.7	−61.3	−9.6
ΔH_f (sextet−quartet)	−6.6[b]	−49.5[b]	−53.1[b]	−1.4[b]

[a] The data taken from ref 13. Thermochemical data were derived by assuming a simple additivity scheme based on Cooks' method. [b] Energy difference between the dissociation limit of the sextet state and the generated fragment species of the quartet state.

TABLE 3: Computed k_H/k_D Values for the H(D) Atom Abstractions via TS_{1-1} in Path 1 and TS_{2-1} in Path 2 and for the Methyl Migration via TS_{3-1} in Path 3; The Spin State Is a Sextet

	T (K)	CH_3OH/CD_3OD	CH_3OH/CD_3OH	CH_3OH/CH_3OD
	200	14.948	1.253	11.935
	250	9.009	1.206	7.495
	300	6.516	1.175	5.557
TS_{1-1}	350	5.186	1.153	4.515
	400	4.386	1.135	3.879
	450	3.851	1.121	3.448
	500	3.476	1.109	3.143
	200	34.408	25.928	1.330
	250	17.856	14.676	1.219
	300	11.468	9.945	1.156
TS_{2-1}	350	8.264	7.430	1.114
	400	6.413	5.915	1.087
	450	5.227	4.918	1.066
	500	4.412	4.210	1.050
	200	6.903	3.583	1.933
	250	4.926	2.893	1.706
	300	3.799	2.456	1.552
TS_{3-1}	350	3.054	2.137	1.434
	400	2.542	1.898	1.346
	450	2.178	1.716	1.274
	500	1.914	1.575	1.219

the moment of inertia I, the vibrational partition function q computed using the harmonic oscillator approximation, and the activation energy E. Moreover, the subscripts H-form mean the complex consisting of FeO^+ and CH_3OH and the subscripts D-form mean the complex consisting of FeO^+ and D-labeled methanol such as CD_3OD, CD_3OH, and CH_3OD. The last exponential term is dominant in this equation because the other terms can be almost all canceled between denominators and numerators. The numerator in the last exponential term comes from the fact that C−H dissociation has a lower activation energy than C−D dissociation on account of the former's greater zero-point vibrational energy.

Table 3 summarizes computed values of k_H/k_D for the electronic processes via **TS_{1-1}** in Path 1, **TS_{2-1}** in Path 2, and **TS_{3-1}** in Path 3 of the sextet state as a function of temperature. Kinetic isotope effect is in general significantly dependent on temperature, so one should specify temperature conditions in discussing reaction mechanisms from measured k_H/k_D values. Since **TS_{1-1}** is responsible for the H atom abstraction of the OH group of methanol, CD_3OD and CH_3OD should undergo larger kinetic isotope effects in this electronic process than CD_3OH. On the other hand, CD_3OD and CD_3OH should have large kinetic isotope effects compared to CH_3OD in the electronic process via **TS_{2-1}** in which one of the H atoms of the methyl group is abstracted. Relatively small isotope effects are observed in the electronic process via **TS_{3-1}** in which the migration of the methyl group takes place. We believe that these theoretical analyses should give a straight answer with respect to the reaction mechanism for the conversion of methanol to formaldehyde. Since **TS_{1-1}** and **TS_{2-1}** have high imaginary frequencies and their potential energy barriers are very thin, a tunneling effect should be important in the vicinity of the transition states. When we make tunneling effect corrections,[32] we expect that the KIE values should be larger than the values in Table 3, depending on the shapes of the potential energy surfaces. New results will be reported in due course.

Conclusions

We have demonstrated from DFT computations at the B3LYP level of theory how the C−H, O−H, and C−O bonds of methanol are activated by an iron−oxo species, FeO^+. The energetics for the oxidation of methanol to formaldehyde should cause the well-known problem of overoxidation in catalytic reactions of alkanes by transition-metal oxides. Produced alcohols are not stable in the presence of an excess of the oxidant and should be further oxidized to aldehydes, carboxylic acids, ketones, and carbon oxides. We computed and analyzed three possible reaction pathways. In Path 1, the H atom of the OH group of methanol is first abstracted by the oxo group of FeO^+ via a four-centered transition state (**TS_{1-1}**) leading to the intermediate complex $HO-Fe^+-OCH_3$, and after that one of the H atoms of the OCH_3 group is shifted to the OH ligand via a five-centered transition state (**TS_{1-2}**) giving the final product complex $H_2O-Fe^+-OCH_2$. In Path 2, one of the H atoms of the CH_3 group of methanol is abstracted by the oxo group via a five-centered transition state (**TS_{2-1}**) leading to the intermediate complex $HO-Fe^+-OHCH_2$, and then the H atom of the $OHCH_2$ group is shifted to the OH ligand via a four-centered transition state (**TS_{2-2}**) giving the product complex. Unlike Paths 1 and 2, which involve a hydrogen shift, the first step in Path 3 involves a methyl migration that takes place via a four-centered transition state (**TS_{3-1}**) resulting in the formation of the intermediate complex $HO-Fe^+-OCH_3$ and the second half of Path 3 is identical to that of Path 1. From B3LYP computations, Path 1 and Path 2 are competitive in energy and Path 3 is energetically unfavorable in comparison with Path 1 and Path 2. We computed and analyzed kinetic isotope effects (k_H/k_D) for the electronic processes of **TS_{1-1}**, **TS_{2-1}**, and **TS_{3-1}**. These theoretical analyses should be useful in considering the reaction mechanism for the conversion of methanol to formaldehyde by FeO^+ as well as other transition-metal oxides.

Acknowledgment. K.Y. is grateful to a Grant-in-Aid for Scientific Research on the Priority Area "Molecular Physical Chemistry" from the Ministry of Education, Science, Sports and Culture of Japan for its support of this work. Computational time was provided by the Supercomputer Laboratory of Kyoto University and by the Computer Center of the Institute for Molecular Science.

Supporting Information Available: Figures of optimized structures of the quartet state. This material is available free of charge via the Internet at http://pubs.acs.org.

References and Notes

(1) (a) Muzart, J. *Chem. Rev.* **1992**, *92*, 113. (b) Lee, D. G.; Gai, H. *Can. J. Chem.* **1993**, *71*, 1394. (c) Hudlicky, M. *Oxidations in Organic*

Chemistry; American Chemical Society: Washington, 1990; ACS Monographf 186. (d) Augustine, R. L.; Trecker, D. J. *Oxidation*; Marcel Dekker: New York, 1971. (e) Stewart, R. In *Oxidation in Organic Chemistry*; Wiberg, K. B., Ed.; Academic Press: New York, 1965; Part A.

(2) Huang, S.; Holman, R. W.; Gross, M. L. *Organometallics* **1986**, *5*, 1857.

(3) Weissermel, K.; Arpe, H.-J. *Industrial Organic Chemistry*, 3rd ed.; VCH: Weinheim: New York, 1997; Chapter 2.

(4) (a) Beden, B.; Leger, J.-M.; Lamy, C. In *Modern Aspects of Electrochemistry*; Bockris, J. O. M., Conway, B. E., White, R. E., Eds.; Plenum: New York, 1992; Vol. 22, p 97. (b) Parsons, R.; Vanernoot, T. *J. Electroanal. Chem*. **1988**, *257*, 9. (c) Reddington, E.; Sapienza, A.; Gurau, B.; Viswanathan, R.; Sarangapani, S.; Smotkin, E. S.; Mallouk, T. E. *Science* **1998**, *280*, 1735.

(5) (a) Yoon, H.; Stouffer, M. R.; Dubt, P. J.; Burke, F. P.; Curran, G. P. *Energy Pgrog*. **1985**, *5*, 78. (b) Cheng, W. H.; Kung, H. H. In *Methanol Production and Use*; Cheng, W. H., Kung, H. H., Eds.; Marcel Dekker: New York, 1994; Chapter 1.

(6) (a) Childers, C. L.; Huang, H.; Korzeniewski, C. *Langmuir* **1999**, *15*, 786. (b) Korzeniewski, C.; Childers, C. L. *J. Phys. Chem. B* **1998**, *102*, 489.

(7) Parr, R. G.; Yang, W. *Density Functional Theory of Atoms and Molecules*; Clarendon: Oxford, 1988.

(8) Schröder, D.; Schwarz, H. *Angew. Chem., Int. Ed. Engl*. **1995**, *34*, 1973.

(9) (a) Schröder, D.; Schwarz, H. *Angew. Chem., Int. Ed. Engl*. **1990**, *29*, 1433. (b) Schröder, D.; Fiedler, A.; Hrusák, J,; Schwarz, H. *J. Am. Chem. Soc.* **1992**, *114*, 1215. (c) Schröder, D.; Schwarz, H.; Clemmer, D. E.; Chen, Y.-M.; Armentrout, P. B.; Baranov, V. I.; Böhme, D. K. *Int. J. Mass Spectrom. Ion Processes* **1997**, *161*, 175.

(10) (a) Schröder, D.; Schwarz, H. *Helv. Chim. Acta* **1992**, *75*, 1281. (b) Becker, H.; Schröder, D.; Zummack, W.; Schwarz, H. *J. Am. Chem. Soc.* **1994**, *116*, 1096. (c) Ryan, M. F.; Stöckigt, D.; Schwarz, H. *J. Am. Chem. Soc*. **1994**, *116*, 9565.

(11) *Chem. Eng. News* **1993**, *29*, 1433.

(12) For the methane-methanol conversion: (a) Yoshizawa, K.; Shiota, Y.; Yamabe, T. *Chem. Eur. J.* **1997**, *3*, 1160. (b) Yoshizawa, K.; Shiota, Y.; Yamabe, T. *J. Am. Chem. Soc.* **1998**, *120*, 564. (c) Yoshizawa, K.; Shiota, Y.; Yamabe, T. *Organometallics* **1998**, *17*, 2825. (d) Yoshizawa, K.; Shiota, Y.; Yamabe, T. *J. Chem. Phys.* **1999**, *111*, 538. For the benzene-phenol conversion: (e) Yoshizawa, K.; Shiota, Y.; Yamabe, T. *J. Am. Chem. Soc.* **1999**, *121*, 147.

(13) Schröder, D.; Wesendrup, R.; Schalley, C. A.; Zummack, W.; Schwarz, H. *Helv. Chim. Acta* **1996**, *79*, 123.

(14) Allison, J.; Ridge, D. P. *J. Am. Chem. Soc.* **1979**, *101*, 4998.

(15) Weil, D. A.; Wilkins, C. L. *J. Am. Chem. Soc.* **1985**, *107*, 7316.

(16) Huang, S.; Holman, R. W.; Gross, M. L. *Organometallics* **1986**, *5*, 1857.

(17) (a) Blum, O.; Stöckigt, D.; Schröder, D.; Schwarz, H. *Angew. Chem., Int. Ed. Engl*. **1992**, *31*, 603. (b) Schalley, C. A.; Wesendrup, R.; Schröder, D.; Weiske, T. Schwarz, H. *J. Am. Chem. Soc*. **1995**, *117*, 7711. (c) Fiedler, A.; Schröder, D.; Schwarz, H.; Tjelta, B. L.; Armentrout, P. B. *J. Am. Chem. Soc*. **1996**, *118*, 5047. (d) Wesendrup, R.; Schalley, C. A.; Schröder, D.; Schwarz, H. *Organometallics* **1996**, *15*, 1435.

(18) (a) Becke, A. D. *Phys. Rev. A* **1988**, *38*, 3098. (b) Becke, A. D. *J. Chem. Phys.* **1993**, *98*, 5648.

(19) Lee, C.; Yang, W.; Parr, R. G. *Phys. Rev. B* **1988**, *37*, 785.

(20) Vosko, S. H.; Wilk, L.; Nusair, M. *Can. J. Phys*. **1980**, *58*, 1200.

(21) Wachters, A. J. H. *J. Chem. Phys*. **1970**, *52*, 1033.

(22) Raghavachari, K.; Trucks, G. W. *J. Chem. Phys*. **1989**, *91*, 1062.

(23) Krishnan, R.; Binkley, J. S.; Seegar, R.; Pople, J. A. *J. Chem. Phys.* **1980**, *72*, 650.

(24) Frisch, M. J.; Trucks, G. W.; Schlegel, H. B.; Scuseria, G. E.; Robb, M. A.; Cheeseman, J. R.; Zakrzewski, V. G.; Montgomery, J. A.; Stratmann, R. E.; Burant, J. C.; Dapprich, S.; Millam, J. M.; Daniels, A. D.; Kudin, K. N.; Strain, M. C.; Farkas, O.; Tomasi, J.; Barone, V.; Cossi, M.; Cammi, R.; Mennucci, B.; Pomelli, C.; Adamo, C.; Clifford, S.; Ochterski, J.; Petersson, G. A.; Ayala, P. Y.; Cui, Q.; Morokuma, K.; Malick, D. K.; Rabuck, A. D.; Raghavachari, K.; Foresman, J. B.; Cioslowski, J.; Ortiz, J. V.; Stefanov, B. B.; Liu, G.; Liashenko, A.; Piskorz, P.; Komaromi, I.; Gomperts, R.; Martin, R. L.; Fox, D. J.; Keith, T.; Al-Laham, M. A.; Peng, C. Y.; Nanayakkara, A.; Gonzalez, C.; Challacombe, M.; Gill, P. M. W.; Johnson, B. G.; Chen, W.; Wong, M. W.; Andres, J. L.; Head-Gordon, M.; Replogle, E. S.; Pople, J. A. *Gaussian 98*; Gaussian Inc.: Pittsburgh, PA, 1998.

(25) Fiedler, A.; Hrusák, J.; Koch, W.; Schwarz, H. *Chem. Phys. Lett.* **1993**, *211*, 242.

(26) Loh, S. K.; Fisher, E. R.; Lian, L.; Schultz, R. H.; Armentrout, P. B. *J. Phys. Chem.* **1989**, *93*, 3159.

(27) Fuhr, J. R.; Martin, G. A.; Wiese, W. L. *J. Phys. Chem. Ref. Data* **1988**, *17*, Suppl. 4.

(28) (a) Fukui, K. *J. Phys. Chem*. **1970**, *74*, 4161. (b) Fukui, K. *Acc. Chem. Res*. **1981**, *14*, 363.

(29) Shaik, S.; Danovich, D.; Fiedler, A.; Schröder, D.; Schwarz, H. *Helv. Chim. Acta* **1995**, *78*, 1393.

(30) The bond distance and the dissociation energy of FeH^+ ($^5\Delta$) are 1.569 Å and 56.9 kcal/mol relative to Fe^+ (^{6}D), respectively, at the B3LYP/6-311G** level of theory. An experimental value for the dissociation energy of FeH^+ ($^5\Delta$) is 48.9 ± 1.4 kcal/mol. For experiment of FeH^+ see: Kickel, B. L.; Armentrout, P. B. In *Organometallic Ion Chemistry*; Freiser, B. S., Ed.; Kluwer: Dordrecht, 1996. For a theoretical calculation of FeH^+ see: Holthausen, M. C.; Koch, W. *Helv. Chim. Acta* **1996**, *79*, 1939; Holthausen, M. C.; Fiedler, A.; Schwarz, H.; Koch, W. *J. Phys. Chem.* **1996**, *100*, 6236.

(31) McQuarrie, D. A. *Statistical Thermodynamics*; University Science Books: Mill Valley, 1973.

(32) Nikitin, E. E. *Theory of Elementary Atomic and Molecular Processes in Gases*; Oxford: Clarendon, 1974.